



## Individual variability in functional connectivity architecture of the mouse brain

Eyal Bergmann <sup>1</sup>, Xenia Gofman<sup>1</sup>, Alexandra Kavushansky<sup>1</sup> & Itamar Kahn <sup>1</sup>✉

In recent years precision fMRI has emerged in human brain research, demonstrating characterization of individual differences in brain organization. However, mechanistic investigations to the sources of individual variability are limited in humans and thus require animal models. Here, we used resting-state fMRI in awake mice to quantify the contribution of individual variation to the functional architecture of the mouse cortex. We found that the mouse connectome is also characterized by stable individual features that support connectivity-based identification. Unlike in humans, we found that individual variation is homogeneously distributed in sensory and association networks. Finally, connectome-based predictive modeling of motor behavior in the rotarod task revealed that individual variation in functional connectivity explained behavioral variability. Collectively, these results establish the feasibility of precision fMRI in mice and lay the foundation for future mechanistic investigations of individual brain organization and pre-clinical studies of brain disorders in the context of personalized medicine.

<sup>1</sup>Department of Neuroscience, Rappaport Faculty of Medicine, Technion – Israel Institute of Technology, Haifa, Israel. ✉email: [kahn@technion.ac.il](mailto:kahn@technion.ac.il)

A fundamental question in brain research is what makes individuals different from each other. This question can be addressed at different levels of organization, starting from genetics or neurotransmitters, going through structural or functional measures of brain regions and networks, and ending at behavioral phenotypes or clinical outcomes. In humans, a common approach to study brain organization in individuals is resting-state functional connectivity magnetic resonance imaging (fcMRI), which estimates functional connectivity between regions based on coherent spontaneous fluctuations in the fMRI signal<sup>1–3</sup>.

Previous human fcMRI studies demonstrated that this measure is stable over time and can be used to characterize individual differences<sup>4–8</sup>. These works revealed that such differences are spread heterogeneously across the human cortex, demonstrating increased variability in association networks, in cortices that underwent expansion and elaboration relative to non-human primates and lower mammals, and in cortices that are characterized by more distal connectivity. Moreover, individual variation in functional connectivity was shown to predict individual activity patterns in task conditions<sup>9,10</sup> and behavioral performance<sup>11–13</sup>. Finally, recent studies in patients with neuropsychiatric disorders reported that individual functional connectivity patterns can be used as a biomarker for diagnosis and treatment optimization<sup>14–16</sup>, key features of personalized medicine.

While individual differences in functional connectivity were thoroughly characterized in humans, including identification of sources of intra-subject variability<sup>17</sup>, a dissection of mechanisms relies on animal models. Such investigation demands an adequate sample size that is hard to achieve in studies in non-human primates and may involve genetic manipulations and molecular techniques that are more readily accessible in rodent models, particularly in mice. Previous fcMRI studies in anesthetized mice demonstrated reproducible resting-state networks<sup>18,19</sup>, applications to mouse models of brain disorders<sup>20–22</sup>, and correlations between functional connectivity and behavioral measures<sup>23–26</sup>. However, characterization of individual differences in functional connectivity is based on repeated data acquisition that can control for measurement instability. Since this experimental design is hard to achieve in anesthetized animals, such studies can benefit from awake mouse imaging. We have previously established fcMRI experiments in awake head-fixed mice<sup>27–29</sup> and used repeated-measurement designs to link individual differences in structural and functional connectivity<sup>30</sup>. However, a detailed analysis of individual variability of functional connectivity in the mouse brain and its relevance to behavior has heretofore not been demonstrated.

Here we used repeated-measurement resting-state fcMRI to characterize individual variation in functional connectivity in the mouse cortex. We show that despite the reduced complexity of the mouse cortex relative to the human homolog and the animals being genetically identical, it is also characterized by individual variation, allowing above chance-level identification of specific mice from a group. Then, we characterize factors affecting identification accuracy, and examine the distribution of individual variability in sensory and association networks. Finally, we link individual differences in functional connectivity to behavioral variability in the accelerating rotating rod task (rotarod), which assesses motor performance. Collectively, these findings indicate that mouse functional networks are characterized by behaviorally relevant individual variation and lay the foundation for future mechanistic investigations of sources of individual variability and pre-clinical studies of brain disorders in the context of personalized medicine.

## Results

**Individual variation in the mouse functional connectome.** Data of the study consisted of nineteen F1 C6/129P (male, age

9–12 weeks), which underwent multiple daily fcMRI sessions during passive wakefulness as previously described<sup>30</sup>, followed by behavioral testing in the rotarod task<sup>31</sup>. After exclusion of sessions with image artifacts or excessive motion (see “Methods”), the final dataset included 16 mice with six sessions (each comprising ~30 min of data), which were split to two halves of three sessions each to examine the group and individual similarities in the mouse functional connectome. For the comparison between functional connectivity and behavior, two additional mice with 4–5 sessions were included. In this analysis, data from all sessions were averaged, resulting in a single connectivity matrix per mouse.

Functional connectivity matrices were built based on the Allen Mouse Brain Atlas (<https://mouse.brain-map.org>)<sup>32</sup> using the Common Coordinate Framework Reference Atlas (CCFv3)<sup>33</sup>. The atlas was downsampled to fMRI resolution (Fig. 1a; mouse-specific images are presented in Supplementary Fig. 1), and included 43 cortical parcels per hemisphere, which were divided into six modules (Prefrontal, Lateral, Somatomotor, Visual, Medial and Auditory) based on anatomical connectivity patterns<sup>34</sup>. The two connectivity matrices of each mouse were compared to each other and to all other connectivity matrices of the other mice (representative matrices are presented in Fig. 1b) by calculating the Fisher’s z-transformed correlations between all edges in the connectome. The resulting network similarity matrix diagonal represents the similarity within individuals, while rows and columns represent similarity between specific mouse and all other mice in the group (Fig. 1c). This matrix was used for quantification of individual variation in the mouse connectome by comparing group and individual network similarities<sup>7</sup>. We found substantial group similarity (mean  $z(r) = 0.9$ ), which indicates that mouse connectomes share a common structure. Nevertheless, we also found that individual similarity (mean  $z(r) = 1.08$ ) is significantly higher than group similarity (two-tailed paired student *t*-test:  $t_{(15)} = 7.32$ ,  $P < 0.001$ , Cohen’s  $d = 1.83$ ), demonstrating substantial differences in 15 out of 16 mice (Fig. 1d), and indicating that fcMRI can capture individual variability in the mouse connectome.

The significant difference between group and individual network similarities means that on average, connectivity matrices from the same mouse are more similar than connectivity matrices from different mice. A more stringent criterion for estimation of individual variation is connectome-based fingerprinting, which tests the ability to accurately identify mice from a group<sup>12</sup>. Such identification means that the similarity between the two connectivity matrices of the same mouse must be higher than the similarity to all other connectivity matrices in the group. To test the feasibility of functional connectome-based fingerprinting in mice, we calculated the fraction of mice in which the values along the diagonal of the similarity matrix were higher than other values in each row and column. We found that the rates of successful identification of mice in the first and second halves of data were 68.75% and 62.5% out of the 16 mice, respectively (Fig. 1e). To formally test the significance of those rates, we used a shuffling procedure, calculated the distribution of identification rates when assigning random identities in either the first or second halves of the connectivity matrices, and found that the observed identification rates are significantly higher than values in all 1000 shuffled iterations ( $P < 0.001$ , Fig. 1e). While the identification rates are more modest than the ones observed in humans (92.9–94.4%)<sup>12</sup>, they nonetheless indicate that individual variability in the mouse connectome is substantial enough to compare between individual connectomes, and distinguish individual connectivity patterns between mice.

A possible confound that may contribute to the estimation of individual variation is head motion. In such case, we expect that mice with increased head motion will have higher individual similarity. An alternative explanation is that mice with higher

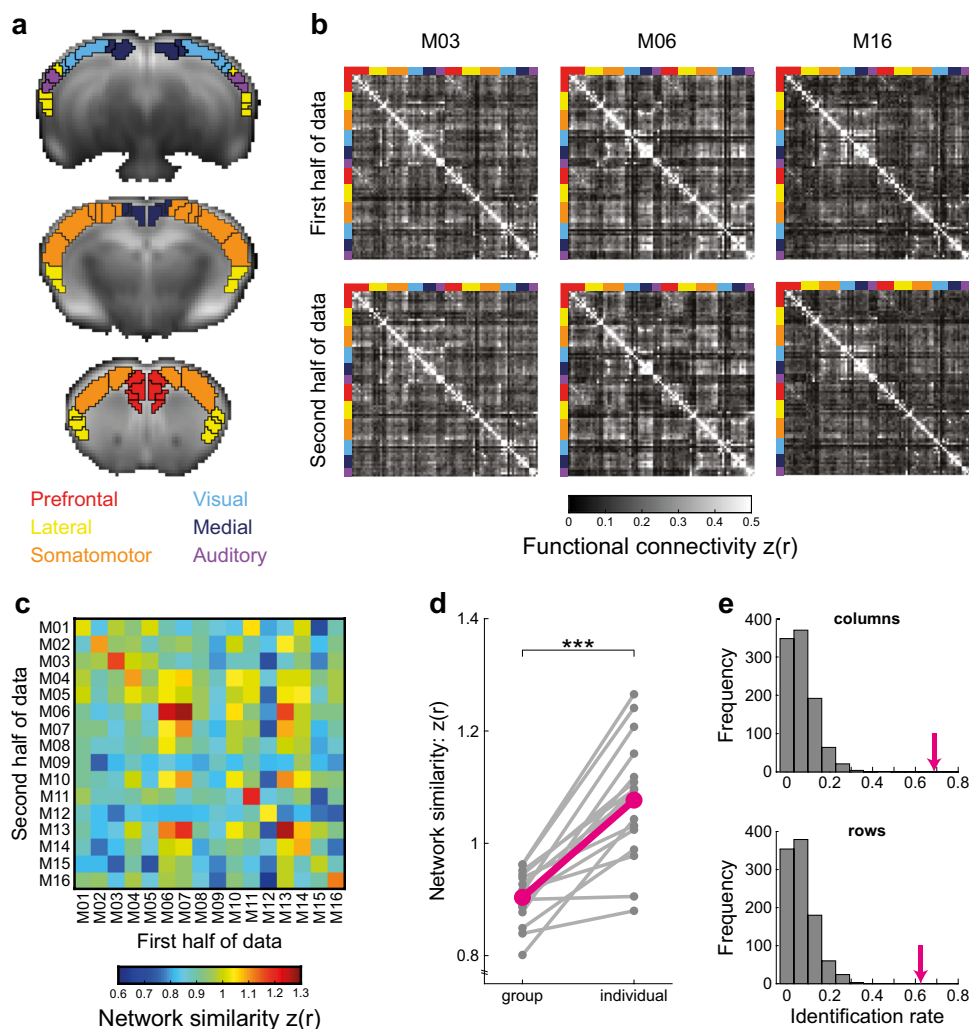


**Fig. 1 Individual variation in the mouse functional connectome.** **a** Anatomical parcellation of the mouse cortex overlaid on average fMRI image at native resolution. Eighty-six cortical labels (black borders) were taken from the Allen Mouse Brain Atlas CCFv3 and divided to six modules (label color) based on their anatomical connectivity profiles<sup>34</sup>. **b** Individual functional connectomes of three representative mice from the cohort demonstrate unique patterns that are consistent between the first and second halves of data. The identity of the anatomical modules of each node is designated by the color. **c** A network similarity matrix in which each cell represents the similarity between two connectomes. The matrix is asymmetric as columns represent the similarity between the first half of data of each mouse and the second half of the data of all the other mice, while rows represent the similarity between the second half of data of each mouse and the first half of data of all the other mice. The values along the diagonal represent individual similarity, which is the correlation between the edges of the two connectivity matrices of the same mouse. **d** A comparison between group and individual similarities demonstrates higher similarity between connectomes from the same mouse ( $n = 16$  mice,  $***P < 0.001$ ), the magenta line depicts the average group and individual network similarities. **e** True connectome-based identification rates (magenta) were compared to 1000 iterations of identity shuffling indicating that individual variation in the mouse functional connectome is substantial enough to enable above chance-level identification of mice from the group.

head motion have less amount of data available for analysis due to motion scrubbing, and as a result will have lower individual similarity. To address this issue, we compared between the average number of frames included after motion scrubbing and the different measures of individual variation, namely group similarity, individual similarity, and identifiability (Supplementary Fig. 2). The results support the second explanation as number of included frames was positively correlated with individual similarity (Spearman correlation:  $\rho_{(14)} = 0.7$ ,  $p = 0.003$ ), but not with group similarity (Spearman correlation:  $\rho_{(14)} = 0.02$ ,  $p = 0.94$ ). Importantly, mice with lower numbers of frames included were less identifiable in the connectome-based fingerprinting analysis. Another control analysis we conducted was to examine whether the estimated individual variation is a result of spurious connections in the connectome (Supplementary Fig. 3). We discovered that applying sparsity thresholds that

constrain the analysis to strong and consistent functional connections that are more anatomically plausible, results in higher estimation of individuality. Finally, to assure that our data acquisition parameters and preprocessing procedure support estimation of individual functional connectivity profiles, we replicated a well-validated quality control measure of functional connectivity specificity<sup>19</sup>, and found that our findings are not driven by mice with non-specific functional connectivity estimates (Supplementary Fig. 4). Collectively, these control analyses suggest that the individual differences observed in the original analysis are not a result of structured noise related to head motion, spurious connections or data quality.

**Factors contributing to characterization of individual variation.** Studies in humans demonstrated that successful identification<sup>12</sup>

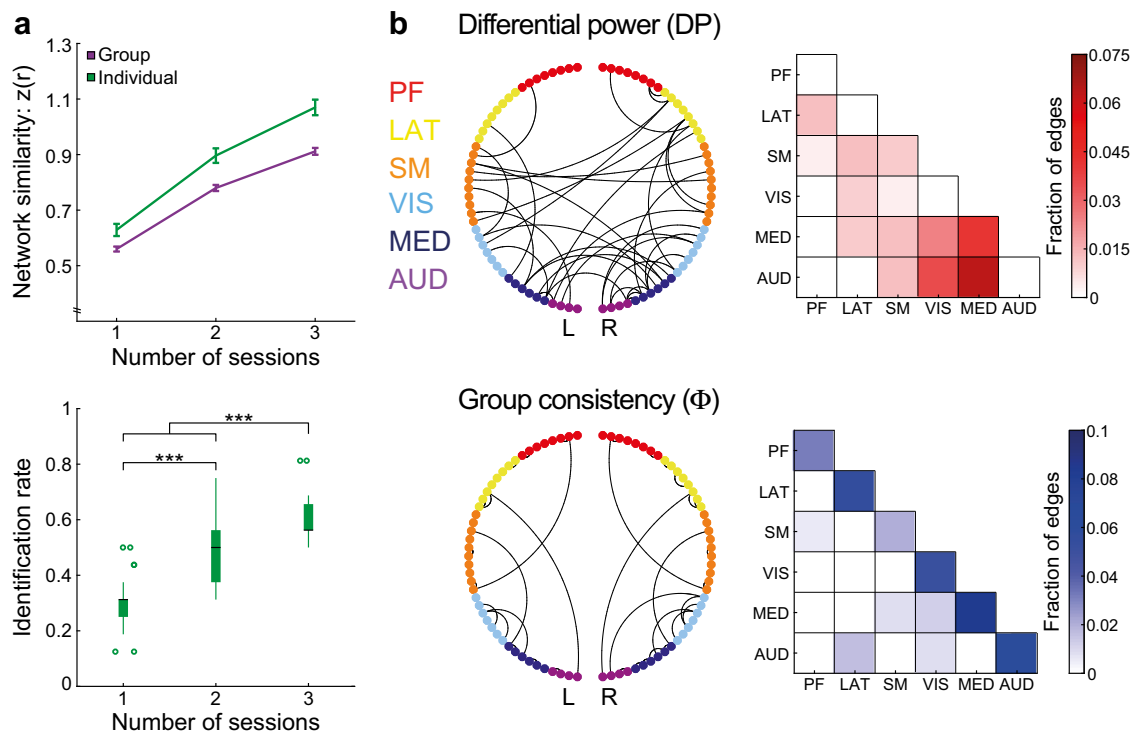


**Fig. 2** Factors contributing to characterization of individual variation. **a** Network similarity values (top) and identification rates (bottom) as a function of number of included sessions in the two connectivity matrices of each mouse. All combinations of data sampling of one, two or three sessions were calculated and compared using repeated-measures ANOVA (network similarity, see text) or two-tailed unpaired student  $t$ -test (identification rate,  $***P < 0.001$ ). Error bars (top) represent the standard error of the mean ( $n = 16$  mice); boxplots (bottom) represent the median (center line), interquartile range (box limits);  $1.5 \times$  interquartile range (whiskers) and outlier (points),  $n = 30$ ,  $n = 90$ ,  $n = 40$  rates derived from connectome-based identification analyses of all combinations of one, two, and three session per half of data, respectively. **b** Unique (DP, top) and consistent ( $\Phi$ , bottom) edges in individual connectomes. For visualization purposes, both measures were thresholded at the 99th percentile. In the circle plot (left) the 86 nodes are organized based on their anatomical module identity and cortical hemisphere; lines indicate edges. In the matrices (right), the fraction of edges connecting between and within modules is color coded, with darkly shaded cells representing higher DP (top) and  $\Phi$  (bottom) values. PF, Prefrontal; LAT, Lateral; SM, Somatomotor; VIS, Visual; MED, Medial; AUD, Auditory.

and precise characterization of individual variation<sup>7</sup> depend on the amount of fcMRI data available per participant. Therefore, leveraging the repeated-measurement design of our fcMRI experiment, we sought to characterize how much data is needed to stably characterize the functional cortical organization in individual mice.

In our original analysis (Fig. 1) two average connectivity matrices were calculated per mouse by splitting its six sessions to two halves, controlling for the total number of included frames per half (see “Methods”). In the current analysis, we built a set of connectivity matrices using all combinations of one ( $n = 15$ ), two ( $n = 45$ ) or three sessions ( $n = 20$ ) per mouse, and examined network similarity and identification rates as a function of the number of sessions averaged per connectome (Fig. 2a). First, we calculated group and individual network similarity values for different number of included sessions and submitted the results to a repeated-measures ANOVA (corrected with the Huynh-Feldt method) with individuality and number of sessions as within mouse factors. We found significant effects of both factors (individuality:  $F_{(1, 15)} = 34.28$ ,  $P < 0.001$ ,  $\epsilon_{H-F} = 1$ ,  $\eta^2 = 0.71$ ; number of sessions:  $F_{(2, 30)} = 7318.76$ ,  $P < 0.001$ ,  $\epsilon_{H-F} = 0.51$ ,  $\eta^2 = 0.998$ ), confirming that network similarity between connectivity matrices from the same mouse is higher than group similarity, and that increasing the amount of data per mouse improves network similarity estimation. Importantly, we also found a significant interaction between individuality and number of sessions ( $F_{(2, 30)} = 109.87$ ,  $P < 0.001$ ,  $\epsilon_{H-F} = 0.5$ ,  $\eta^2 = 0.887$ ), indicating that increasing the amount of data per mouse preferentially increases individual over group network similarity values. In agreement with

this finding, the results of the identification analysis revealed that increasing the number of sessions improve identification (two-tailed unpaired student  $t$ -test: two sessions vs. one session:  $t_{(58)} = 9.08$ ,  $P < 0.001$ , Cohen’s  $d = 2.9$ ; three sessions vs. one session:  $t_{(33)} = 15.53$ ,  $P < 0.001$ , Cohen’s  $d = 5.3$ ; three sessions vs. two sessions:  $t_{(63)} = 8$ ,  $P < 0.001$ , Cohen’s  $d = 2.15$ ). Collectively, these analyses indicate that repeat-measurement fcMRI designs supported by awake imaging are useful for characterizing individual functional connectivity patterns.

After establishing that the mouse functional connectome is characterized by stable individual features, we sought to characterize which brain connections contribute to individual variation. Therefore, we replicated that analysis of Finn et al.<sup>12</sup> and characterized which edges possess high differential power (DP) that contribute to identification, and which edges possess high group consistency ( $\Phi$ ) within mice and across the group. We derived those values for all edges in the connectivity matrix, and determined which edges were in the top 1% of each measure (Fig. 2b). We found that most edges in the top 1% of DP are related to the posterior modules, namely, Visual, Medial, and Auditory, and include many inter-hemispheric and inter-module connections. In contrast, edges in the top 1% of  $\Phi$  came from all modules and included mainly intra-hemispheric intra-module connections. In the original analysis of Finn et al.<sup>12</sup>, high DP were observed in high-order fronto-parietal connections, while high  $\Phi$  were observed in inter-hemispheric connectivity within the Somatomotor and Visual networks. Comparing the analyses across species, we conclude that while the mouse data recapitulate



the  $\Phi$  difference between intra- and inter-module connections, and show DP bias toward specific modules, it seems to not show a difference between sensory and association regions. Therefore, we sought to directly examine individual variation in those qualitatively different brain systems.

**Individual variation across brain systems.** To better characterize individual variation in sensory and association systems in the mouse cortex, we sought to examine whether functional connectivity profiles within these systems differ in their identifiability or group and individual network similarities. Therefore, we defined each cortical node as either sensory (Somatomotor, Visual, and Auditory modules) or association (Prefrontal, Lateral, and Medial modules) and derived two network similarity matrices (Fig. 3a). Then, we calculated group and individual network similarities for each system (Fig. 3b), and found higher values compared to the original full connectivity matrix (all connections) in both group (two-tailed paired student  $t$ -test: all connections vs. association:  $t_{(15)} = 26.9$ ,  $P < 0.001$ , Cohen's  $d = 6.73$ ; all connections vs. sensory:  $t_{(15)} = 18.44$ ,  $P < 0.001$ , Cohen's  $d = 4.61$ ) and individual similarities (all connections vs. association:  $t_{(15)} = 8.92$ ,  $P < 0.001$ , Cohen's  $d = 2.23$ ; all connections vs. sensory:  $t_{(15)} = 11.59$ ,  $P < 0.001$ , Cohen's  $d = 2.9$ ). Comparison between association and sensory systems revealed significant difference in group network similarity ( $t_{(15)} = 4.96$ ,  $P < 0.001$ , Cohen's  $d = 1.24$ ), but no difference in individual network similarity ( $t_{(15)} = 0.56$ ,  $P = 0.583$ , Cohen's  $d = 0.14$ ; all values were corrected for multiple comparison using false-discovery rate

based on the Benjamini–Hochberg method). Examining the normalized relative effect magnitude of individuality (Fig. 3c), we found no difference between sensory and association systems ( $t_{(15)} = 1.803$ ,  $P = 0.137$ , Cohen's  $d = 0.45$ ). Nevertheless, comparison to the full connectivity matrix revealed lower effect magnitude of individuality in association ( $t_{(15)} = 3.02$ ,  $P = 0.026$ , Cohen's  $d = 0.75$ ), but not sensory ( $t_{(15)} = 0.134$ ,  $P = 0.85$ , Cohen's  $d = 0.03$ ), systems. Finally, we carried out the identification analysis for each type of connectome and found similar identification rates in sensory and association systems (Fig. 3d), which were only slightly lower than the original values yielded by the full connectivity matrix. Collectively, these analyses indicate that connections between sensory and association regions, which reflect inter-module connectivity, are less consistent across the group. Importantly, the results indicate that the relative effect magnitude of individuality on functional organization of the mouse cortex is more modest compared to humans<sup>7</sup>, and the qualitative differences between sensory and association networks in the human brain are not well recapitulated in mice.

After characterizing individual variation at the level of cortical network, we sought to examine this measure at a regional level. Therefore, we calculated group and individual similarity for each of the 86 cortical regions (Supplementary Data 1 and Supplementary Fig. 5). We found consistent group and individual similarity values in most regions, except for lower values in posterior areas with lower signal-to-noise ratio (postrhinal area and posterolateral visual area). Importantly, we also found that the normalized relative individual effect magnitude is also varied between different regions. We hypothesized that this variation

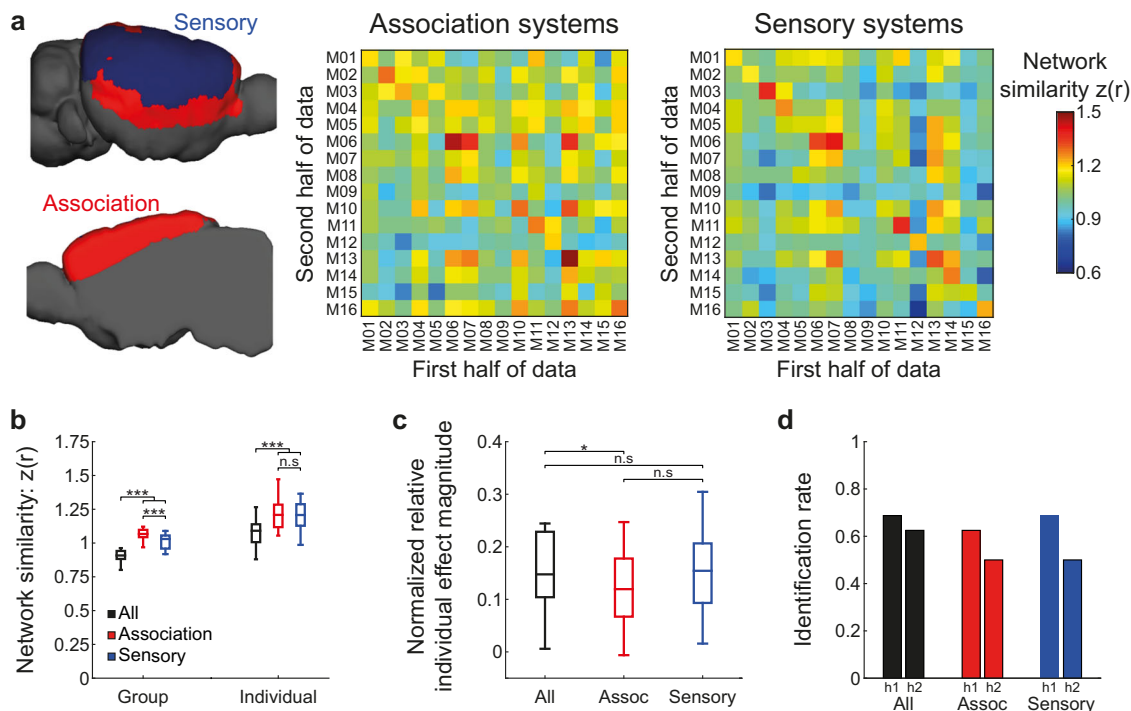


**Fig. 3 Comparison of individual variation between association and sensory cortical systems.** **a** Segmentation of cortical modules to association and sensory networks (left) and the similarity matrices between individual connectomes which were limited to either association or sensory regions (right). **b** Comparison between group and individual similarities of the full connectome (All) and the connectomes built using only association (Assoc) or sensory regions demonstrates that the full connectome is characterized by lower similarity values at both Group and Individual levels ( $n = 16$  mice,  $***P < 0.001$ ). Boxplots represent the median (center line), interquartile range (box limits) and  $1.5 \times$  interquartile range (whiskers). **c** Comparison between normalized relative individual effect magnitude of the different connectomes reveals no difference between sensory and association networks. However, comparison between sensory and association networks to the full connectome revealed lower normalized relative individual effect magnitude only in association networks ( $n = 16$  mice,  $*P < 0.05$ ). **d** Identification rates of individual mice using the three different connectomes, demonstrate slightly increased performance in the full connectome with minimal differences between association and sensory networks. h1, first half of data; h2, second half.

could be explained by the hierarchical organization of the mouse cortex<sup>34</sup>, which might be reflected in differential variability of regions with different proportions of feedforward and feedback connections. However, comparisons between regional normalized effect magnitudes and anatomical hierarchy scores revealed non-significant Spearman correlations (corticocortical hierarchy:  $\rho_{(35)} = -0.21$ ,  $p = 0.2$ ; corticocortical + thalamocortical + corticothalamic hierarchy:  $\rho_{(35)} = -0.26$ ,  $p = 0.12$ ), which is consistent with the homogeneity between sensory and association systems. Nevertheless, this finding may also be explained by the fact that in comparison to anatomical tracing, fcMRI lacks directionality or layer-specificity and is affected also by polysynaptic connectivity.

**Individual brain-behavior relations in mice.** After characterizing individual variation in the functional architecture of the mouse cortex, we sought to examine whether it can predict behavioral phenotypes. Therefore, we used connectome-based predictive modeling (CPM)<sup>35</sup> to link between functional connectivity profiles and behavioral performance in the rotarod task, which is a well-validated test for motor coordination in rodents<sup>31</sup>. In this task, mice are placed on an accelerating horizontal rod and learn to walk forward and not fall off. Examining rotarod performance, we found prominent variability within the group with different mice presenting wide range of latencies to fall (Fig. 4a). This behavioral variability could be predicted by the functional connectivity data using CPM (Fig. 4b) as leave-one-out cross-validation (LOOCV) analysis, in which the rotarod performance of an individual mouse is predicted based on brain-behavior correlations in the rest of the group, demonstrated good correspondence between predicted and observed mean latencies to fall ( $r_{(16)} = 0.51$ ). To formally test the goodness of prediction, we shuffled the behavioral data 1000 times and ran LOOCV analyses on shuffled data to extract significance level ( $P = 0.021$ ), which confirmed significant prediction. Importantly, latency to fall values were not correlated with individual average head motion estimates during scanning ( $r_{(16)} = -0.27$ ,  $P = 0.27$ ), confirming that the prediction is not artifactually increased by motion patterns.

Finally, we explored which functional connections contributed to the model (Fig. 4c) and found that positive correlations were more frequent in edges connecting sensory nodes, while negative correlations were less frequent and characterized mainly edges connecting between sensory and lateral association nodes. To formally test this observation, we used a set of two-tailed Z-tests for independent proportions (Fig. 4d) to test whether significant edges are biased toward connections between association nodes (A:A,  $n = 946$ ), sensory nodes (S:S,  $n = 861$ ) or one sensory and one association node (A:S,  $n = 1848$ , all comparisons were corrected for multiple comparisons using false-discovery rate). This analysis confirms that positive correlations are more frequent in S:S connections than in A:S ( $Z = 5$ ,  $P < 0.001$ ) and A:A ( $Z = 6.07$ ,  $P < 0.001$ ) connections, with additional bias toward A:S relative to A:A connections ( $Z = 2.62$ ,  $P = 0.018$ ). In contrast, negative correlations were more frequent in A:S connections, demonstrating significant bias relative to S:S connections ( $Z = 2.27$ ,  $P = 0.035$ ), and marginally significant bias relative A:A connections ( $Z = 1.87$ ,  $P = 0.073$ ); comparison of A:A and S:S connections revealed no difference ( $Z = 0.95$ ,  $P = 0.34$ ). Collectively, the data establish that fcMRI can be used to characterize individual brain-behavior relations.

## Discussion

In this study, we characterized individual variation in the functional organization of the mouse cortex. We found evidence for stable individual features in the mouse connectome, that allows above chance level identification of individual mice from a group.

Then, we demonstrated that identification rates increase with the amount of data per mouse, indicating that repeated-measurement experimental design is advantageous for precise characterization of mouse-specific connectomes. Comparing individual variation between sensory and association networks, we found that the differences observed between those cortical systems in humans are not well recapitulated in mice. Finally, we show that variance in functional connectivity, especially between sensory cortices, can explain behavioral variability in the rotarod task. Collectively, these findings lay the foundations for studying the functional organization of the mouse brain in health and disease at the level of the individual animal.

While the field of precision fMRI has recently emerged in human brain research<sup>4,7,12,36,37</sup>, rodent data are still analyzed at the group level<sup>19,38</sup>. A major challenge in precision fMRI is the need for extensive amounts of data per subject ranging from 50 to 100 min based on the studied brain structure<sup>39</sup>. This amount of data is not trivial to obtain in anesthetized mice in which acquisition is predominantly between several minutes and up to 40 min per session<sup>40,41</sup> and a substantive repeated-measurement design is challenging due to the difficulties that arise from repeated ventilation and catheterization and the potential impact of prolonged anesthesia, although longitudinal imaging with inter-scan gap of few to several weeks was demonstrated<sup>22</sup>. On the other hand, experimental setups for awake fcMRI<sup>27,42–44</sup> can easily support such repeated-measurement designs. Therefore, despite the controversy on optimal scanning procedure in rodents and the lack of standardization in the field<sup>45</sup>, awake fcMRI is highly useful for precision fcMRI analysis in individual mice.

Comparison between the findings of this work and the two seminal human studies of Finn<sup>12</sup> and Gratton<sup>7</sup> shows that while the central findings of those studies are recapitulated in mice, there are also some important differences. First, identification rates in our mouse cohort are lower and the effect magnitude of individuality is more modest in mice, in which cortical organization is strongly dominated by group shared features. Moreover, the heterogeneity in individual variation among brain networks was not recapitulated in mice, demonstrating similar patterns in sensory and association systems. While these differences might be explained by the complex organization of the human cortex<sup>46</sup>, expansion of association networks in humans<sup>47,48</sup> or qualitative differences in anatomically homologous high-order structures<sup>27</sup>, it is also likely that genetic homogeneity in our cohort reduces the contribution of individual features, as genetics was previously shown to shape functional connectivity<sup>49</sup>. In addition, some differences are perhaps related to the areal parcellation that was used for defining nodes in the connectome. In humans, connectomes defined based on functional areal parcellation resulted in several hundred seed regions<sup>50–53</sup>. Since such algorithms have yet to be adapted to mice, and are beyond the scope of the current work, we used anatomical parcellation based on the Allen Mouse Brain Atlas, which is comprised of 86 cortical labels<sup>33,34</sup>. Previous studies in mice showed close agreement between structural and functional connectivity in the mouse brain<sup>27,54</sup>, including in gross cortical organization<sup>55</sup>. Moreover, using the Allen Mouse Brain Atlas, we have recently shown that structural connectomes can predict their functional counterpart<sup>30</sup>, suggesting that this anatomical parcellation is functionally relevant. However, a major limitation of using the Allen Mouse Brain Atlas is mouse-specific variability in areal organization or geometric deformation in the registration process, that may bias connectivity matrices from the same mouse to be more similar. While we cannot exclude such bias as controlling for it analytically is difficult, it does not explain why individual similarity increases with the amount of data per mouse. Further, restricting the connectivity matrices to anatomically plausible connections replicates the result, suggesting that

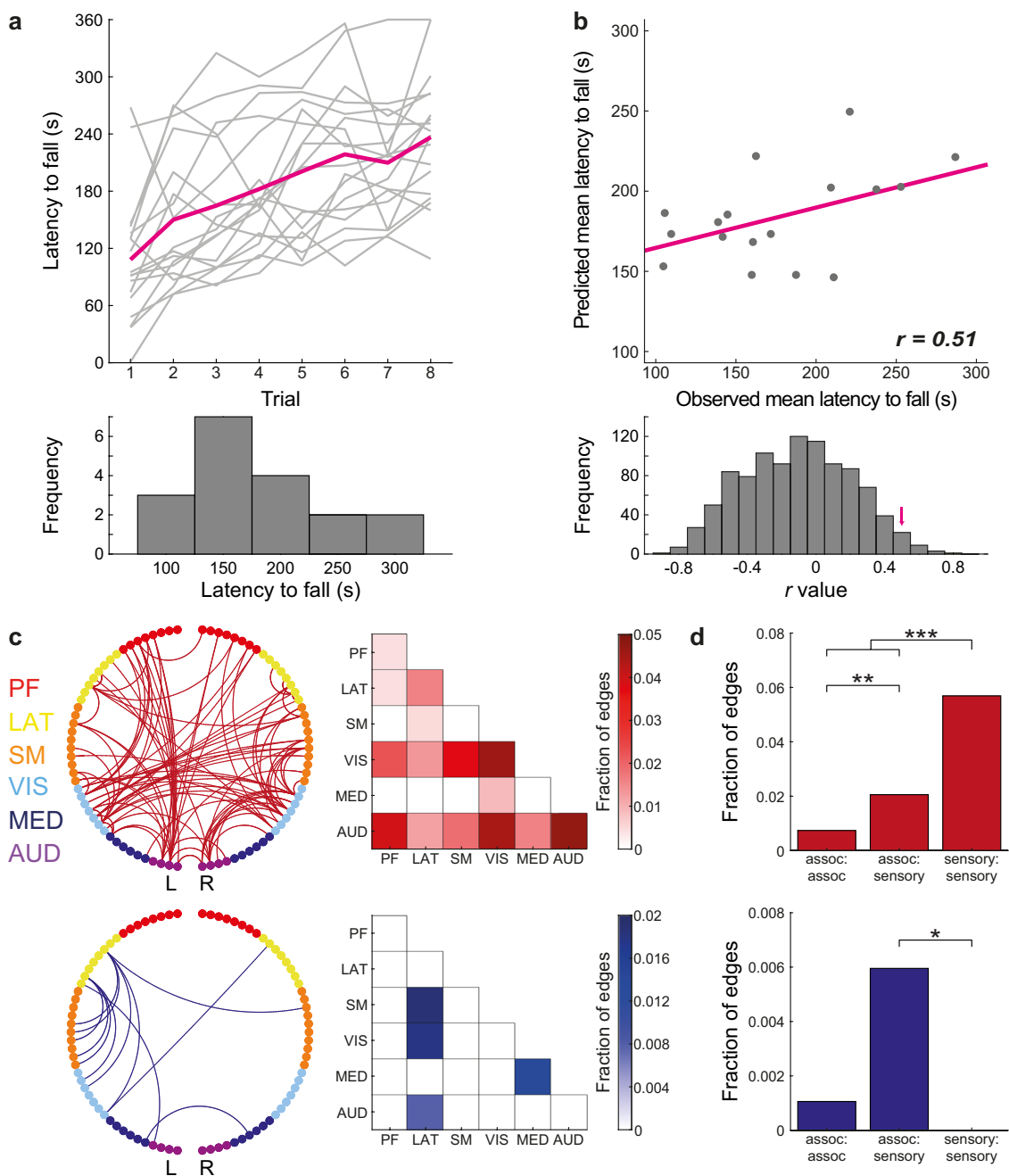


**Fig. 4** Connectome-based predictive modeling of individual performance in the rotarod task. **a** Individual (light gray) and group average (magenta) performance in the rotarod task (top), demonstrate considerable variability in the mean latency to fall of different mice in the group (bottom). **b** Relations between observed and predicted mean latency to fall values ( $n = 18$  mice) show close agreement (top). A formal statistical analysis was done using a shuffling analysis in which connectome-based predictive modeling was applied to shuffled rotarod data, the original  $r$ -value (magenta arrow) designates the 21 highest value out of 1000 iterations. **c** Circle plot (left) and matrix (right) representations of edges that were positively (red, top) or negatively (blue, bottom) correlated with rotarod performance in all leave-one-out cross-validation iterations. **d** All edges from the previous analysis were divided to three categories: connections between two association regions (assoc:assoc,  $n = 946$ ), connections between an association and a sensory region (assoc:sensory,  $n = 1848$ ) and connections between two sensory regions (sensory:sensory,  $n = 861$ ). The results revealed that edges which are positively correlated with the task are biased to sensory:sensory connections (red, top), while edges that are negatively correlated with the task are slightly biased to association: sensory connections ( $*P < 0.05$ ,  $**P < 0.01$ ,  $***P < 0.001$ ). PF, Prefrontal; LAT, Lateral; SM, Somatomotor; VIS, Visual; MED, Medial; AUD, Auditory.

a major biological component contributes to individual variation. Importantly, it is unlikely that registration issues will result in variations that predict behavior in a leave-one-out cross-validation analysis such as CPM.

An important aspect of this study is the link between individual variation in functional connectivity and behavioral variability in

the rotarod task. While CPM is a well-validated approach in humans<sup>35</sup>, it is usually implemented on a large cohorts ( $N > 100$ ), although Rosenberg et al.<sup>13</sup> were able to predict sustained attention in a group of 31 participants. Here, we used a repeated-measurement design to collect large amount of data per mouse, allowing us to successfully implement a CPM analysis in a group

of 18 mice with correlation between predicted and observed behavior that is comparable to the results of the previous reports in humans<sup>12,13,56</sup>. The contributing edges in our model involve mainly sensory nodes, which are expected to support motor learning. Surprisingly, the contributing edges do not involve many connections within the somatomotor system, but connections of this system to visual and auditory regions, which may facilitate multisensory integration required for balance. While the whole brain correlates of the rotarod task were not well-studied, structural MRI revealed that rotarod training is related to reduced fractional anisotropy in the visual cortex. Additionally, the visual cortex is known to encode running-related locomotion signals<sup>57</sup>. Finally, vestibular stimulation is known to activate somatomotor, visual and auditory cortices<sup>58</sup>, thus shared vestibular signals may explain the role of the connectivity of those regions in behavioral variability. Collectively, the findings suggest that such multisensory integration is required for performance in the rotarod task, but better characterization of the role of auditory and visual areas in the task, as well as causal manipulation of their activity are needed to better understand their exact role in motor coordination.

A major limitation of precision fMRI in humans is the restriction to one level of analysis, as it is limited to large-scale organization<sup>59</sup>. As a result, it is hard to link individual variation in functional connectomes to brain function and dysfunction. In contrast, tools available in rodents support causal manipulation of brain activity using molecular techniques such as chemogenetics or optogenetics, which can be combined with fMRI<sup>41,60–64</sup>. However, heretofore such analyses were restricted to the group level. Future studies can use the individual functional connectome to predict the effect of causal control similar to the way human resting-state fMRI is used to predict individual task fMRI activation pattern<sup>9</sup>, linking the different levels of organization and uncovering sources of individual variation. In addition, rodent models of disease are commonly studied using fcMRI<sup>21,22,29,65</sup>, which allows direct translation to humans<sup>20,28</sup>, as well as studying the relations between functional connectivity and behavior<sup>23–26</sup>. Such studies can utilize the approach presented here to follow the trajectory of individual animals during development, aging or after treatment, as well as CPM, which provides a data-driven alternative for fcMRI-based behavioral prediction<sup>35</sup>, rather than the hypothesis-driven approach that examines the behavioral correlations of specific functional connections.

Together, our results establish the feasibility of the precision fMRI approach in studying the mouse functional connectome, indicating that individual variation in the organization of cortical networks is likely to extend across the mammalian class in general, and is not restricted to primates. Given this foundation, future mouse fMRI studies can follow the human neuroimaging community by moving from group-level inferences to the level of the individual animal. Such transition can be highly beneficial for mechanistic investigation of brain organization, as well as for pre-clinical studies of neuropsychiatric disorders in the context of personalized medicine.

## Methods

**Mice, surgical procedures, behavioral training.** All procedures were conducted in accordance with the ethical guidelines of the National Institutes of Health and were approved by the institutional animal care and use committee (IACUC) at Technion. A detailed description of the experimental design was previously published<sup>30</sup>. Briefly, 19 first generation B6129PF/J1 hybrid mice (males, 9–12 weeks old) were implanted with MRI-compatible head-posts and housed in reversed 12 h light/dark cycle. Then, acclimatized to awake fMRI during passive wakefulness over 4 sessions (2, 5, 10, and 25 min)<sup>27</sup> and underwent seven 45 min long awake imaging sessions over 7–12 days ( $9.94 \pm 1.59$ , mean  $\pm$  SD), followed by one structural MRI session under anesthesia (not used in the current

study). Three days after MRI data were acquired, mice underwent a 2-day rotarod testing.

**Image acquisition.** MRI scans were performed at 9.4 Tesla MRI (Bruker BioSpin GmbH, Ettlingen, Germany) using a quadrature 86 mm transmit-only coil and a 20 mm loop receive-only coil (Bruker); Raw fMRI data were reconstructed using ParaVision 5.1 (Bruker). Each awake fMRI session started with a brief anesthesia (5% isoflurane) to allow proper mounting to the custom-made cradle<sup>27</sup>. Mice typically were alert within less than a minute. Mice had ~15 min to fully recover from the anesthesia during scanner calibrations and acquisition of a short low-resolution rapid acquisition process with a relaxation enhancement (RARE) T1-weighted structural image (TR = 1500 ms, TE = 8.5 ms, RARE-factor = 4, FA = 180°, 30 coronal slices,  $150 \times 150 \times 450 \mu\text{m}^3$  voxels, no interslice gap, FOV  $19.2 \times 19.2 \text{ mm}^2$ , matrix size of  $128 \times 128$ ). Then, four spin-echo echo-planar imaging (SE-EPI) runs were acquired (TR = 2500 ms, TE = 18.398 ms, 200 time points, FA = 90°, 30 coronal slices,  $150 \times 150 \times 450 \mu\text{m}^3$  voxels, no interslice gap, FOV  $14.4 \times 9.6 \text{ mm}^2$ , matrix size of  $96 \times 64$ ) before mice were returned to their home cages.

**Rotarod.** To assess general motor function, we used the accelerating rotating rod task (rotarod)<sup>31</sup> in which mice (up to five at once) walk on a rotating rod (ENV-575MA, Med Associates, St. Albans, VT) while the speed of rotation is accelerating from 4 to 40 rounds per minute during a period of 6 min. Each mouse was trained for two consecutive days over four trials per day with an inter trial interval of 15 min. The latency between the beginning of each trial and falling time was calculated to extract individual learning curves and later averaged across trials to extract a single value for overall task performance per mouse.

**MRI data preprocessing.** Functional data were preprocessed as previously described<sup>27,28,30</sup> including removal of the first two frames for T1-equilibration effects, compensation for slice-dependent time shifts, rigid body motion correction, registration to a downsampled version of the Allen Mouse Brain Atlas (AMBC CCFv3, available at <https://mouse.brain-map.org>)<sup>32,33</sup> using session-specific low-resolution anatomical scan and high-resolution anatomical template (see supplementary Fig. 1 in Bergmann et al.<sup>27</sup>), and intensity normalization. At this stage, one mouse was excluded due to susceptibility artifacts in the parietal cortex, and additional three sessions were also excluded due to ghosting artifacts in the EPI.

After this general fMRI preprocessing, an fcMRI-specific preprocessing was performed. First, data underwent motion scrubbing to remove motion-related artifacts<sup>66</sup>. Censoring criteria were frame displacement of  $50 \mu\text{m}$  and temporal derivative root mean square variance over voxels of 150% inter-quartile range above the 75th percentile, with an augmented mask of one additional frame after each detected movement and censoring of sequences with less than five included frames. Runs with less than 50 frames and sessions with less than 192 frames (8 min) were excluded (a total of six sessions). The average number of included sessions per mouse was  $6.33 \pm 0.84$  (mean  $\pm$  SD) and the average total included time per session was  $19.31 \pm 3.67$  min per session. After motion scrubbing, preprocessing continued with demeaning and detrending, nuisance regression of six motion parameters, ventricular and white matter signals, and their first derivatives, temporal filter ( $0.009 < f < 0.08 \text{ Hz}$ ), and spatial smoothing (Gaussian kernel with FWHM of  $450 \mu\text{m}$ ).

**Construction of the functional connectome.** To construct the functional connectome of each mouse, we used the AMBC Atlas to define 86 regions in the mouse cortex (43 per hemisphere), which were classified into six different modules (Prefrontal, Lateral, Somatomotor, Visual, Medial, and Auditory) based on their anatomical connectivity patterns<sup>34</sup>. Labels were registered to the native fMRI resolution using the nearest neighbor interpolation<sup>67,68</sup>. The very deep and superficial aspects of each label were removed to minimize partial-volume effects. In addition, posterior parts of the retrosplenial and primary visual cortices were also removed due to inconsistent registration in these areas.

After defining connectome nodes, we extracted their time courses in each session of each mouse and calculated the Fisher's z-transformed Pearson correlation ( $r$ ) values<sup>69</sup>, resulting in an  $86 \times 86$  connectivity matrix per session. Then, these matrices were split to two halves of three sessions per mouse for similarity and identification analyses (minimizing the difference in number of included frames per half) or averaged across all sessions of each mouse for the connectome-based predictive modelling (CPM) analysis. Mice with less than six valid sessions ( $n = 2$ ) were included only in the CPM analysis. In mice with seven valid sessions ( $n = 9$ ), the session with the highest head motion was excluded from the similarity and identification analyses in order to match the amount of data per half.

**Similarity and identification analyses.** To quantify individual variation and perform connectome-based fingerprinting/identification, we adapted algorithms developed in humans to estimate network similarity<sup>7</sup> and identification rates<sup>12</sup>. Both procedures are based on the construction of a similarity matrix, in which each cell is the Fisher's z-transformed correlation between values in all 3655 edges in two connectomes, columns represent the first half of data and rows represent the



second half of data. For quantification of network similarity, values along the diagonal represent individual similarity, which is the correlation between the connectomes built for the same mouse from the two halves of data. Group similarity is defined as the average of values in a combined row and column vector (excluding the value along the diagonal). The identification procedure is a more stringent analysis that quantifies the fraction of mice in which the individual similarity is higher than any other value in each row or column.

To test whether individual variation differs between association and sensory networks in the mouse cortex, we constructed connectomes limited to either association ( $n = 44$ ) or sensory ( $n = 42$ ) modules. Then, we ran the similarity and identification analyses as described. Additionally, we calculated the normalized relative individual effect magnitude, which is the added similarity of individual connectome over group connectomes, calculated by subtracting group similarity from individual similarity and dividing by the latter.

Parcel-level individual variation was estimated similarly by comparing the functional connectivity profiles of each of the 86 cortical regions. For estimation of normalized relative effect magnitude of individuality, negative similarity values were rounded to 0.001, and then normalized relative effect magnitudes of individuality that were negative were rounded to zero. To compare parcel-level similarity to anatomical hierarchical scores taken from the supplementary materials in the work of Harris et al.<sup>34</sup>, the normalized relative effect magnitudes were averaged between the two cortical hemispheres.

#### Quantifying the amount of data needed to study individual variation in mice.

To characterize the amount of data needed for studying individual variation in mice, we examined the effects of the number of sessions included in the construction of each connectome on network similarity and identification rate. We built two connectomes per mouse using one, two or three sessions per connectome, and examined all possible combinations. Similarity values were averaged between the combinations of the different sessions per mouse, while identification rates were extracted per combination. Then, we replicated the similarity and identification analyses described above.

**Quantifying edgewise contributions to identification.** Edge-based analyses examine which connections contribute more to successful identification. A detailed description of the calculation of group consistency ( $\Phi$ ) and differential power (DP) was previously published<sup>12</sup>. Briefly, each connectome underwent  $z$ -normalization, and the edgewise product was calculated for each edge in all pairs of connectomes. Group consistency values are the average edgewise products from the comparisons of the two connectomes of each mouse. In contrast, DP represents the empirical probability that the edgewise product of two connectomes from the same mouse is higher than the edgewise product of two connectomes from different mice. The top 1% of DP and  $\Phi$  were presented in either circle plots or matrix plots grouped to modules<sup>35</sup>.

**Connectome-based predictive modelling (CPM).** To link individual variation in the functional connectome to behavioral variability in the rotarod task, we followed a previously published detailed protocol for CPM<sup>35</sup>. We used a leave-one-out cross-validation approach in which Spearman correlation was calculated between functional connectivity in each edge in the connectome and rotarod mean latency to fall values for  $n - 1$  mice over 18 iterations. In each iteration, significant ( $P < 0.05$ , uncorrected) positive and negative correlations were selected and summarized to two values per mouse, which were combined in a single regression model. This model was used for prediction of rotarod performance in the  $n^{\text{th}}$  testing mouse in each one of the 18 iterations. Finally, the correlation between predicted and observed rotarod performance, which is statistically independent of the edge selection threshold, was calculated and formally tested by comparing it to the distribution of correlation in 1000 iterations in which rotarod mean latency to fall values were randomly assigned to mice<sup>35</sup>. To characterize the edges that contributed to the prediction, we extracted the edges that were included in the model in all 18 iterations and presented them in both circle and matrix plots and examined whether the contributing edges were biased to connections between association or sensory regions.

**Statistics and reproducibility.** Group and individual similarity values ( $n = 16$ ) were compared using paired student  $t$ -test or repeated-measures ANOVA after normality was tested using the Lilliefors test. Statistical analysis for connectome-based identification ( $n = 16$ ) and connectome-based predictive modelling ( $n = 18$ ) was done using shuffling analysis with 1000 iterations in which animals' identities were randomly assigned before calculating identification rates or correspondence between predicted and observed rotarod performance. The rank of the observed values compared to the sorted shuffled values was used to determine statistical significance.

The effects of number of included sessions on estimation of network similarity and identification rates were examined using repeated-measures ANOVA or two-tailed unpaired student  $t$ -test, respectively.

A set of  $Z$ -tests for independent proportions was used to compare the distribution of contributing edges in the CPM analysis between sensory and association regions.

#### Data availability

Imaging raw data in this study are available in BIDS format on OpenNeuro, <https://openneuro.org/datasets/ds002307>.

#### Code availability

MRI data were preprocessed using SPM2 and FSL. Data analysis was conducted in MATLAB (Mathworks) using the Statistics and Machine Learning toolbox code. Network similarity was calculated using a custom-written code available on OpenNeuro (<https://openneuro.org/datasets/ds002307>). Codes for identification and connectome-based predictive modeling adapted from the work of Finn et al.<sup>12</sup> and Shen et al.<sup>35</sup> which were previously published: <https://www.nitrc.org/projects/bioimagesuite>. The circular graphs were generated using P. Kassebaum's (2020) circle plots (<https://www.github.com/paul-kassebaum-mathworks/circularGraph>).

Received: 15 April 2020; Accepted: 11 November 2020;

Published online: 04 December 2020

#### References

1. Fox, M. D. & Raichle, M. E. Spontaneous fluctuations in brain activity observed with functional magnetic resonance imaging. *Nat. Rev. Neurosci.* **8**, 700–711 (2007).
2. Buckner, R. L., Krienen, F. M. & Yeo, B. T. Opportunities and limitations of intrinsic functional connectivity MRI. *Nat. Neurosci.* **16**, 832–837 (2013).
3. Power, J. D., Schlaggar, B. L. & Petersen, S. E. Studying brain organization via spontaneous fMRI signal. *Neuron* **84**, 681–696 (2014).
4. Gordon, E. M. et al. Precision functional mapping of individual human brains. *Neuron* **95**, 791–807.e7 (2017).
5. Kong, R. et al. Spatial topography of individual-specific cortical networks predicts human cognition, personality, and emotion. *Cereb. Cortex* **29**, 2533–2551 (2019).
6. Mueller, S. et al. Individual variability in functional connectivity architecture of the human brain. *Neuron* **77**, 586–595 (2013).
7. Gratton, C. et al. Functional brain networks are dominated by stable group and individual factors, not cognitive or daily variation. *Neuron* **98**, 439–452.e5 (2018).
8. Laumann, T. O. et al. Functional system and areal organization of a highly sampled individual human brain. *Neuron* **87**, 657–670 (2015).
9. Tavor, I. et al. Task-free MRI predicts individual differences in brain activity during task performance. *Science* **352**, 216–220 (2016).
10. Cole, M. W., Ito, T., Bassett, D. S. & Schultz, D. H. Activity flow over resting-state networks shapes cognitive task activations. *Nat. Neurosci.* **19**, 1718–1726 (2016).
11. Smith, S. M. et al. A positive-negative mode of population covariation links brain connectivity, demographics and behavior. *Nat. Neurosci.* **18**, 1565–1567 (2015).
12. Finn, E. S. et al. Functional connectome fingerprinting: identifying individuals using patterns of brain connectivity. *Nat. Neurosci.* **18**, 1664–1671 (2015).
13. Rosenberg, M. D. et al. A neuromarker of sustained attention from whole-brain functional connectivity. *Nat. Neurosci.* **19**, 165–171 (2015).
14. Drysdale, A. T. et al. Resting-state connectivity biomarkers define neurophysiological subtypes of depression. *Nat. Med.* **23**, 28–38 (2017).
15. Boerwinkle, V. L. et al. Network-targeted approach and postoperative resting-state functional magnetic resonance imaging are associated with seizure outcome. *Ann. Neurol.* **86**, 344–356 (2019).
16. Abraham, A. et al. Deriving reproducible biomarkers from multi-site resting-state data: An Autism-based example. *Neuroimage* **147**, 736–745 (2017).
17. Poldrack, R. A. et al. Long-term neural and physiological phenotyping of a single human. *Nat. Commun.* **6**, 8885 (2015).
18. Gozzi, A. & Schwarz, A. J. Large-scale functional connectivity networks in the rodent brain. *Neuroimage* **127**, 496–509 (2016).
19. Grandjean, J. et al. Common functional networks in the mouse brain revealed by multi-centre resting-state fMRI analysis. *Neuroimage* **205**, 116278 (2020).
20. Bertero, A. et al. Autism-associated 16p11.2 microdeletion impairs prefrontal functional connectivity in mouse and human. *Brain* **141**, 2055–2065 (2018).
21. Grandjean, J. et al. Complex interplay between brain function and structure during cerebral amyloidosis in APP transgenic mouse strains revealed by multi-parametric MRI comparison. *Neuroimage* **134**, 1–11 (2016).
22. Zerbi, V. et al. Dysfunctional autism risk genes cause circuit-specific connectivity deficits with distinct developmental trajectories. *Cereb. Cortex* **28**, 2495–2506 (2018).
23. Pagani, M. et al. Deletion of autism risk gene Shank3 disrupts prefrontal connectivity. *J. Neurosci.* **39**, 5299–5310 (2019).

24. Michetti, C. et al. The knockout of synapsin II in mice impairs social behavior and functional connectivity generating an ASD-like phenotype. *Cereb. Cortex* **27**, 5014–5023 (2017).
25. Liska, A. et al. Homozygous loss of autism-risk gene CNTNAP2 results in reduced local and long-range prefrontal functional connectivity. *Cereb. Cortex* **28**, 1141–1153 (2018).
26. Ash, J. A. et al. Functional connectivity with the retrosplenial cortex predicts cognitive aging in rats. *Proc. Natl Acad. Sci. USA* **113**, 12286–12291 (2016).
27. Bergmann, E., Zur, G., Bershadsky, G. & Kahn, I. The organization of mouse and human cortico-hippocampal networks estimated by intrinsic functional connectivity. *Cereb. Cortex* **26**, 4497–4512 (2016).
28. Shofty, B. et al. Autism-associated Nfl deficiency disrupts corticocortical and corticostriatal functional connectivity in human and mouse. *Neurobiol. Dis.* **130**, 104479 (2019).
29. Asleh, J. et al. Brain-wide structural and functional disruption in mice with oligodendrocyte-specific Nfl deletion is rescued by inhibition of nitric oxide synthase. *Proc. Natl Acad. Sci. USA* **117**, 22506–22513 (2020).
30. Mellozzi, F. et al. Individual structural features constrain the mouse functional connectome. *Proc. Natl Acad. Sci. USA* **116**, 26961–26969 (2019).
31. Deacon, R. M. J. Measuring motor coordination in mice. *J. Vis. Exp.* e2609 (2013).
32. Lein, E. S. et al. Genome-wide atlas of gene expression in the adult mouse brain. *Nature* **445**, 168–176 (2007).
33. Wang, Q. et al. The allen mouse brain common coordinate framework: A 3D Reference Atlas. *Cell* **181**, 936–953.e20 (2020).
34. Harris, J. A. et al. Hierarchical organization of cortical and thalamic connectivity. *Nature* **575**, 195–202 (2019).
35. Shen, X. et al. Using connectome-based predictive modeling to predict individual behavior from brain connectivity. *Nat. Protoc.* **12**, 506–518 (2017).
36. Sylvester, C. M. et al. Individual-specific functional connectivity of the amygdala: a substrate for precision psychiatry. *Proc. Natl Acad. Sci. USA* <https://doi.org/10.1073/pnas.1910842117> (2020).
37. Greene, D. J. et al. Integrative and network-specific connectivity of the basal ganglia and thalamus defined in individuals. *Neuron* **105**, 742–758.e6 (2019).
38. Zerbi, V., Grandjean, J., Rudin, M. & Wenderoth, N. Mapping the mouse brain with rs-fMRI: An optimized pipeline for functional network identification. *Neuroimage* **123**, 11–21 (2015).
39. Gratton, C. et al. Defining individual-specific functional neuroanatomy for precision psychiatry. *Biol. Psychiatry* **88**, 28–39 (2020).
40. Gutierrez-Barragan, D., Basson, M. A., Panzeri, S. & Gozzi, A. Infralow state fluctuations govern spontaneous fMRI network dynamics. *Curr. Biol.* **29**, 2295–2306.e5 (2019).
41. Zerbi, V. et al. Rapid reconfiguration of the functional connectome after chemogenetic locus coeruleus activation. *Neuron* **103**, 702–718.e5 (2019).
42. Yoshida, K. et al. Physiological effects of a habituation procedure for functional MRI in awake mice using a cryogenic radiofrequency probe. *J. Neurosci. Methods* **274**, 38–48 (2016).
43. Liang, Z., King, J. & Zhang, N. Anticorrelated resting-state functional connectivity in awake rat brain. *Neuroimage* **59**, 1190–1199 (2012).
44. Tsurugizawa, T. et al. Awake functional MRI detects neural circuit dysfunction in a mouse model of autism. *Sci. Adv.* **6**, eaav4520 (2020).
45. Mandino, F. et al. Animal functional magnetic resonance imaging: trends and path toward standardization. *Front. Neuroinform.* **13**, 78 (2020).
46. Glasser, M. F. et al. A multi-modal parcellation of human cerebral cortex. *Nature* **536**, 171–178 (2016).
47. Buckner, R. L. & Krienen, F. M. The evolution of distributed association networks in the human brain. *Trends Cogn. Sci.* **17**, 648–665 (2013).
48. Krubitzer, L. In search of a unifying theory of complex brain evolution. *Ann. N. Y. Acad. Sci.* **1156**, 44–67 (2009).
49. Glahn, D. C. et al. Genetic control over the resting brain. *Proc. Natl Acad. Sci. USA* **107**, 1223–1228 (2010).
50. Power, J. D. et al. Functional network organization of the human brain. *Neuron* **72**, 665–678 (2011).
51. Shen, X., Tokoglu, F., Papademetris, X. & Constable, R. T. Groupwise whole-brain parcellation from resting-state fMRI data for network node identification. *Neuroimage* **82**, 403–415 (2013).
52. Craddock, R. C., James, G. A., Holtzheimer, P. E., Hu, X. P. & Mayberg, H. S. A whole brain fMRI atlas generated via spatially constrained spectral clustering. *Hum. Brain Mapp.* **33**, 1914–1928 (2012).
53. Gordon, E. M. et al. Generation and Evaluation of a Cortical Area Parcellation from Resting-State Correlations. *Cereb. Cortex* **26**, 288–303 (2016).
54. Stafford, J. M. et al. Large-scale topology and the default mode network in the mouse connectome. *Proc. Natl Acad. Sci. USA* **111**, 18745–18750 (2014).
55. Grandjean, J., Zerbi, V., Balsters, J. H., Wenderoth, N. & Rudin, M. Structural Basis of Large-Scale Functional Connectivity in the Mouse. *J. Neurosci.* **37**, 8092–8101 (2017).
56. Beaty, R. E. et al. Robust prediction of individual creative ability from brain functional connectivity. *Proc. Natl Acad. Sci. U. S. A.* **115**, 1087–1092 (2018).
57. Saleem, A. B., Ayaz, A. I., Jeffery, K. J., Harris, K. D. & Carandini, M. Integration of visual motion and locomotion in mouse visual cortex. *Nat. Neurosci.* **16**, 1864–1869 (2013).
58. L Leong, A. T. et al. Optogenetic fMRI interrogation of brain-wide central vestibular pathways. **116**, 10122–10129 (2019).
59. D’Esposito, M. Are individual differences in human brain organization measured with functional MRI meaningful? *Proc. Natl Acad. Sci. USA* **116**, 22432–22434 (2019).
60. Grandjean, J. et al. A brain-wide functional map of the serotonergic responses to acute stress and fluoxetine. *Nat. Commun.* **10**, 350 (2019).
61. Desai, M. et al. Mapping brain networks in awake mice using combined optical neural control and fMRI. *J. Neurophysiol.* **105**, 1393–1405 (2011).
62. Lee, J. H. et al. Global and local fMRI signals driven by neurons defined optogenetically by type and wiring. *Nature* **465**, 788–792 (2010).
63. Weitz, A. J. et al. Thalamic input to orbitofrontal cortex drives brain-wide, frequency-dependent inhibition mediated by GABA and zona incerta article thalamic input to orbitofrontal cortex drives brain-wide, frequency-dependent inhibition mediated by GABA and zona incerta. *Neuron* **104**, 1153–1167.e4 (2019).
64. Bernal-Casas, D., Lee, H. J., Weitz, A. J. & Lee, J. H. Studying brain circuit function with dynamic causal modeling for optogenetic fMRI. *Neuron* **93**, 522–532.e5 (2017).
65. Sforazzini, F. et al. Altered functional connectivity networks in acallosal and socially impaired BTBR mice. *Brain Struct. Funct.* **221**, 941–954 (2014).
66. Power, J. D. et al. Methods to detect, characterize, and remove motion artifact in resting state fMRI. *Neuroimage* **84**, 320–341 (2014).
67. Jenkinson, M. & Smith, S. A global optimisation method for robust affine registration of brain images. *Med. Image Anal.* **5**, 143–156 (2001).
68. Jenkinson, M., Bannister, P., Brady, M. & Smith, S. Improved optimization for the robust and accurate linear registration and motion correction of brain images. *Neuroimage* **17**, 825–841 (2002).
69. Zar, J. H. *Biostatistical Analysis*. (Prentice Hall, 1996).

## Acknowledgements

This research was supported by Israel Science Foundation (770/17), the Ministry of Science & Technology, Israel & Ministry of Europe and Foreign Affairs (MEAE) and the Ministry of Higher Education, Research and Innovation (MESRI) of France, the Adelis Foundation, and the Prince Center. We thank Technion’s Biological Core Facilities and Edith Suss-Toby for her assistance with MRI, and the Technion Preclinical Research Authority, and Nadav Cohen for assistance with animal care.

## Author contributions

E.B. and I.K. designed the study; E.B. collected the MRI data; A.K. collected the rotarod data; E.B. and X.G. analyzed the data; E.B. and I.K. prepared the paper.

## Competing interests

The authors declare no competing interests.

## Additional information

**Supplementary information** is available for this paper at <https://doi.org/10.1038/s42003-020-01472-5>.

**Correspondence** and requests for materials should be addressed to I.K.

**Reprints and permission information** is available at <http://www.nature.com/reprints>

**Publisher’s note** Springer Nature remains neutral with regard to jurisdictional claims in published maps and institutional affiliations.



**Open Access** This article is licensed under a Creative Commons Attribution 4.0 International License, which permits use, sharing, adaptation, distribution and reproduction in any medium or format, as long as you give appropriate credit to the original author(s) and the source, provide a link to the Creative Commons license, and indicate if changes were made. The images or other third party material in this article are included in the article’s Creative Commons license, unless indicated otherwise in a credit line to the material. If material is not included in the article’s Creative Commons license and your intended use is not permitted by statutory regulation or exceeds the permitted use, you will need to obtain permission directly from the copyright holder. To view a copy of this license, visit <http://creativecommons.org/licenses/by/4.0/>.

© The Author(s) 2020